Strength of aluminium alloy ship plating under combined shear and compression/tension

M.S. Syrigou, S.D. Benson & R.S. Dow
Newcastle University, Newcastle Upon Tyne, UK

ABSTRACT: This study investigates the failure modes, ultimate strength and post collapse behaviour of unstiffened aluminium plates under combined loads of shear and axial compression/tension. A non-linear finite element method is used to model simply supported plates with restrained and unrestrained edges. The generated stress/strain curves and the interaction diagrams for combined shear and axial compression/tension loads are presented for a range of different plate slenderness ratios and two marine grade aluminium alloys: 5083-H116 and 6082-T6. This study has been carried out with the aim of incorporating the effect of shear and torsion into the simplified progressive collapse method, which is a well-established approach for assessing the ultimate strength of a hull girder. The existing method is applied to ship hull girders under an assumed pure longitudinal hogging and sagging bending moment. Extending this method to incorporate the effects of shear and torsion will improve its capability for the analysis of intact and damaged ship structures built from steel and aluminium where shear and torsion may be significant.

1 INTRODUCTION

The ultimate strength of a ship is normally defined by the capacity of the main hull girder under longitudinal hogging and sagging bending moment. Several methods are available to evaluate the ultimate strength and compare to the extreme wave induced loading. These include the simplified progressive collapse method (also known as the incremental-iterative method in some classification rules) and nonlinear finite element method. Both these methods normally consider pure longitudinal bending moment as the principal load case. However, particularly in the case of damage, longitudinal bending may not be the governing load condition. Torsion and shear forces may appreciably influence the global strength. Therefore the effect of combined loading is an important factor to be investigated.

Longitudinal bending of a hull girder generates axial compression/tension on the longitudinally effective structure. Torsion loads on the hull girder are resisted by the cellular cross section of the girder. This principally results in shear forces acting on the continuous plating. Therefore combined global bending and torsion on the hull girder causes combined axial compression/tension and shear loads on the local plate structure.

Using a nonlinear finite element method (NLFEM), we investigate the failure modes, ultimate strength and post collapse behaviour of unstiffened aluminium plates under combined shear and axial compression/tension. Results for steel plates have previously been published Syrigou et al., (2014). The results are compared to existing analytical methods to predict combined ultimate strength and the parameters which affect the pre and post collapse response of the plate are defined.

The outcome is presented in a useful format with the aim of incorporating shear and torsion into the simplified progressive collapse method Smith, (1977). The extension of this method to account for different load effects will be particularly useful in a damage scenario, where a quick estimation of residual strength is essential during recoverability and survivability decision making.

2 BACKGROUND

The behaviour of steel plates under axial compression and tension with typical geometry equivalent to ship structures has been examined thoroughly in the literature. For example, Faulkner, (1975) derived a highly effective design formula (based on the Frankland formula) for predicting the ultimate strength of a long plate, which captures elasto-plastic collapse of stocky plate and post buckling strength of more slender plating. Test data are presented in several studies, for example by Frieze et al., (1977). Chalmers,

(1993) presents typical load shortening curves for plates over a range of non-dimensional slenderness which can be used effectively in incremental progressive collapse methods.

Steel plates subjected to shear are less thoroughly examined by Paik & Thayamballi, (2003), Eurocode 3 ENV 1993-1-1, (2005), Alinia et al., (2009), Rizzo et al., (2014) and Zhang et al., (2008) and there is very limited research in plates under combined compressive/tensile and shear loads Harding et al., (1977). The parameters which affect their behaviour are the shape and the level of initial imperfections and also the level of weld induced residual stresses which may be present in a ship-type plate.

However, the outcome of the research for steel plates cannot be applied directly to equivalent aluminium alloy plates. Both the load shortening curves and ultimate strength of aluminium plates under axial compression differ from those for steel plates due to the different material stress-strain curve and the influence of the heat affected zone where material close to a joint is softened due to the high heat input during welding Benson, (2011).

Marine grade aluminium alloy plates subjected to in-plane loads were investigated experimentally by Mofflin, (1983). Benson, (2011) compared Mofflin's results with empirical formulas suggested by Faulkner, (1975), Johnson-Ostenfeld (DNV, 2001), Eurocode 9 EN 1997-1-1, (2007) and Paik and Duran, (2004). The comparison has shown a very good correlation of all for low (equal/less than 1) and intermediate (1 to 2.3) slenderness ratio (β) but not for higher values.

To extend this comparison, we compare the results from this study for unrestrained and restrained aluminium alloy plates under axial compression/tension with the following empirical formulas:

- Faulkner's formula for steel unwelded and unconstrained plates Faulkner, (1975):

$$\frac{\sigma}{\sigma_o} = \frac{2}{\beta} + \frac{1}{\beta^2}, \beta \geq 1 \quad (1)$$

where σ_o = proof yield stress at 0.2% offset strain; β = plate slenderness ratio, defined as:

$$\beta = b/t\sqrt{\sigma_o / \mathrm{E}} \quad (2)$$

where b = plate breadth; t = plate thickness; and E = Young's modulus.

- Eurocode 9 class 4 for marine alloys Eurocode 9 EN 1997-1-1, (2007) :

$$\frac{N_{ED}}{N_{Rd}} \leq 1.0 \quad (3)$$

where N_{ED} = design value of the compression force; N_{Rd} = design resistance to normal forces equal to:

$$N_{Rd} = \frac{A_{eff} \cdot \sigma_o}{\gamma_{M1}} \quad (4)$$

For the purposes of comparison with other theoretical formulas, we assume $N_{ED} = N_{Rd}$; γ_{M1} = safety factor to account design uncertainties is taken equal to 1. Hence:

$$N_{Rd} = A_{eff} \cdot \sigma_o \quad (5)$$

where σ_o = proof yield stress at 0.2% offset strain; A_{eff} = overall effective area equal to:

$$A_{eff} = 2b_{HAZ}\rho_{0HAZ}t + (b - 2b_{HAZ})\rho_C t \quad (6)$$

where b_{HAZ} = width of the Heat Affected Zone; t = plate thickness. The reduced factors of the yield stress in the HAZ and of the proof yield stress are:

$$\rho_{0HAZ} = \frac{\sigma_{0HAZ}}{\sigma_0} \quad (7)$$

$$\rho_C = \frac{C_1}{\left(\frac{\beta}{\varepsilon}\right)} - \frac{C_2}{\left(\frac{\beta}{\varepsilon}\right)^2} \quad (8)$$

where $C_1 = 29$; $C_2 = 198$

$$\beta = \frac{b}{t} \quad (9)$$

$$\varepsilon = \sqrt{250/\sigma_0} \quad (10)$$

- Paik and Duran's (Paik and Duran, 2004):

$$\frac{\sigma}{\sigma_0} = \begin{Bmatrix} -0.13\beta + 0.921, & \beta < 3 \\ -0.07\beta + 0.741, & \beta \geq 3 \end{Bmatrix} \quad (11)$$

where σ_o = proof yield stress at 0.2% offset strain; β = plate slenderness ratio, defined in equation 2.

As concern, aluminium plates subjected to pure shear Eurocode 9 EN 1997-1-1, (2007) provides the following formulas:

$$V_{ED} \leq V_{Rd} \quad (12)$$

where V_{ED} = design value of the shear force at the cross section; V_{Rd} = design shear resistance of the cross section. For the purposes of comparison with our results, we assume $V_{ED} = V_{Rd}$, which for:

- Non-slender plates $\beta \leq 39\varepsilon$, where β is defined by (9) and ε by (10), yielding check is required using the formula:

$$V_{Rd} = A_{net} \cdot \sigma_o / \left(\sqrt{3}\right)\gamma_{M1} \quad (13)$$

where γ_{M1} = safety factor to account design uncertainties is taken equal to 1 for the comparison; A_{net} = net effective area equal to:

$$A_{net} = 2b_{HAZ}.\frac{\sigma_{HAZ}}{\sigma_o}\cdot t + \left(b - 2b_{HAZ}\right)\frac{\sigma_o}{\sigma_o}t \quad (14)$$

- Slender plates $\beta > 39\varepsilon$, where β is defined by (9) and ε by (10), yielding check is required the equation (13) and buckling check using the following formula:

$$V_{Rd} = \nu_1 \cdot b \cdot t \cdot \sigma_o / \left(\sqrt{3}\right)\gamma_{M1} \quad (15)$$

where γ_{M1} = safety factor to account design uncertainties is taken equal to 1 for the comparison; and ν_1 equal to:

$$\nu_1 = 17 \cdot t \cdot \varepsilon \cdot \sqrt{k_\tau}\,/\,b \quad (16)$$

but less than:

$$\nu_1 = k_\tau \frac{430 \cdot t^2 \cdot \varepsilon^2}{b^2} \text{ and } \nu_1 \le 1 \quad (17)$$

where b = plate's breadth; a = plate's length; and if $\alpha/b \ge 1$, $k\tau$ derives from:

$$k_\tau = 5.34 + 4.00 \cdot \left(b/a\right)^2 \quad (18)$$

We have previously investigated the behaviour of simply supported square steel plates under combined axial compressive and shear loads (Syrigou et al., 2014). These results have already been validated; therefore we apply the same approach to model aluminium alloys 5083-H116 and 6082-T6 taking into account the particularities of the material.

3 FINITE ELEMENT PLATE MODEL

3.1 *Plate characteristics*

In this study, aluminium alloys 5083-H116 and 6082-T6 square plates 1000x1000mm with typical slenderness ratio values β = 1 to 6 are modelled in ABAQUS CAE non-linear finite element software. The finite element mesh is modelled using quadrilateral shell elements with reduced integration (S4R). A Heat Affected Zone (HAZ) of 25mm each has been considered along the 2 sides of the plate based on Benson's research (Benson, 2011). A mesh element size of 10x10mm is chosen after mesh convergence study.

The material properties of aluminium alloys 5083-H116 and 6082-T6 are proof yield stress $\sigma_{0.2}$=215MPa and $\sigma_{0.2}$=260MPa respectively, Young's modulus E=70GPa and ν=0.33. The stress-strain curves were obtained from the Ramberg-Osgood model approximation (Ramberg and Osgood, 1943) using 'knee factor' (n) equal to 15 for aluminium alloy 5083-H116 and 30 for aluminium alloy 6082-T6 in the following equation:

$$\varepsilon = \frac{\sigma}{\mathrm{E}} + 0.002\left(\frac{\sigma}{\sigma_{0.2}}\right)^n \quad (19)$$

The reduced stress in the HAZ was calculated for aluminium alloy 5083-H116 and 6082-T6 respectively as:

- $\sigma_{Y_{HAZ}} = 0.67 \cdot \sigma_{0.2} = 0.67 \cdot 215 = 144.05 MPa$
- $\sigma_{Y_{HAZ}} = 0.53 \cdot \sigma_{0.2} = 0.53 \cdot 260 = 130.91 MPa$

The same Ramberg-Osgood relationship with the same knee factor was used for the heat affected material as used for the parent metal.

Additionally, the tensile stress was assumed equal to $0.95\sigma_{YHAZ}$ in each 25mm HAZ and the longitudinal residual stresses were incorporated in the plates.

Finally, the imperfections of the plate were comprised of single half sine wave distributions in both directions in order to incorporate a realistic distortion of the critical elastic buckling mode with average level of initial imperfection amplitude:

$$w_o = 0.1\beta^2 t \quad (20)$$

3.2 *Boundary conditions*

A complex set of boundary conditions had to be developed to adequately cope with the combinations of shear and in-plane applied loads on the plate. They are defined as follows (with reference to Fig. 1):

3.2.1 *Initial condition*

- Edge 1 is fixed in x, y, z
- Edge 2, 3 & 4 are fixed in y
- Edge 3 is constrained in x in order all the nodes to have the same displacement
- Edge 2:
  - Unrestrained edge: Linearity in z of the nodes between RP1and RP4.
  - Restrained edge: Linearity in z and x of the nodes between RP1and RP4.
- Edge 4:
  - Unrestrained edge: Linearity in z of the nodes between RP2 and RP3.
  - Restrained edge: Linearity in z and x of the nodes between RP2and RP3.

3.2.2 *Relaxation step*

The residual stress is modelled using initial stress conditions at every section point in the mesh. This can cause slight departure from equilibrium because it is combined with initial imperfections. Therefore an intermediate step without load precedes the load

step in order to ensure self-equilibrating stress distribution.

3.2.3 *Load*

The Riks arc length method is used to increment the load application, which is carried out with displacement control on Edge 3 in:

- z direction for axial compression/tension
- x direction for shear
- z and x direction simultaneously for combined loads of axial compression/tension and shear.

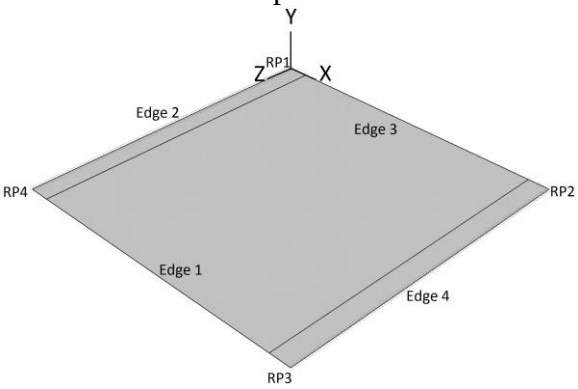

Figure 1. Finite Element model of square plate.

4 RESULTS

4.1 *Alloy 5083-H116*

The load shortening curves of unrestrained and restrained plates are shown in Figure 2 and 3 respectively.

The very stocky plates (β=1) under axial compression are independent from the boundary conditions on the unloaded edges of the plate, i.e. unrestrained or restrained, so there is no change in their ultimate strength. However, the behaviour of slender plates alters due to the boundary conditions. Restrained plates have higher ultimate strength and stiffness in comparison with the unrestrained plates. This phenomenon becomes stronger as the plate becomes more slender.

The restrained plates which are subjected to tension present also higher stress and stiffness in comparison with the unrestrained but almost at the same level all plates, independently their slenderness ratio (β).

Figure 4 and 5 show the shear stress-shear strain curves for unrestrained and restrained plates. The behaviour of the stocky plates (β=1 & β=2) is not affected by the different boundary conditions on the unloaded edges of the plate. Slender plates, β=3-6, present gradual reduction in their critical shear stress in both cases but with higher levels of critical shear stress and stiffness for the restrained plates in comparison with the corresponding unrestrained.

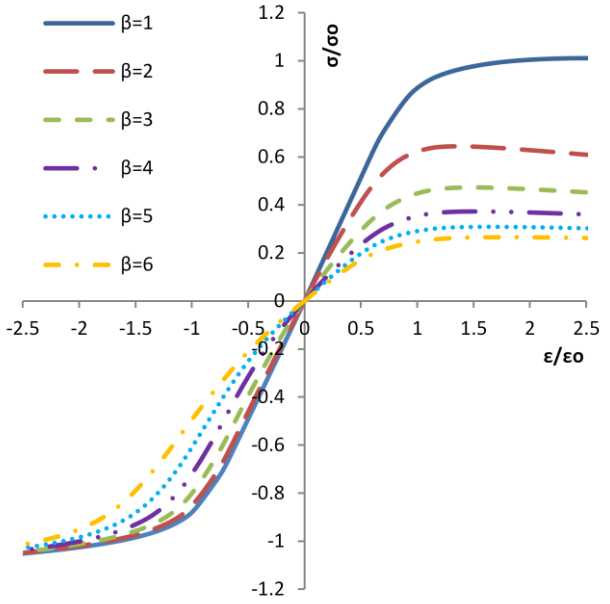

Figure 2. Stress-strain curves of aluminium alloy 5083-H116 plates with unrestrained edges under axial compression/tension.

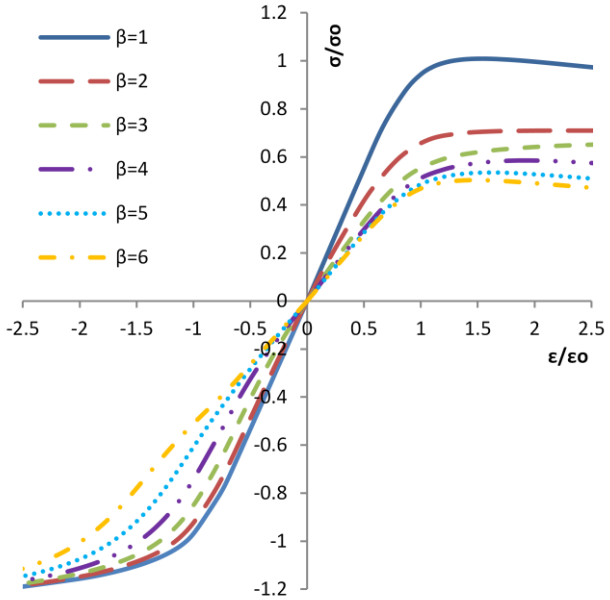

Figure 3. Stress-strain curves of aluminium alloy 5083-H116 plates with restrained edges under axial compression/tension.

The ultimate strength of unrestrained and restrained plates under axial compression is compared with Faulkner's (1), Eurocode 9 (4) and Paik and Duran's (11) theoretical formulas in Figure 6. The graph of the F.E. results for the unrestrained plates shows a good correlation with Faulkner's and Eurocode 9 results. The graph of the stocky F.E. restrained plates has the same tendency but it alters for slender plates. Paik and Duran's graph for slender plates is close to Faulkner's, Eurocode 9 and the F.E. graph for unrestrained plates, but with different slope. Stocky plates (β=1, 2) are not particularly affected by the boundary conditions of the unloaded edges. The restrained slender plates sustain higher values of direct stress in comparison with the unrestrained. This behaviour is expected and agrees with other studies for

steel plates, Harding's (Harding et al., 1977) and the authors' previous study (Syrigou et al., 2014).

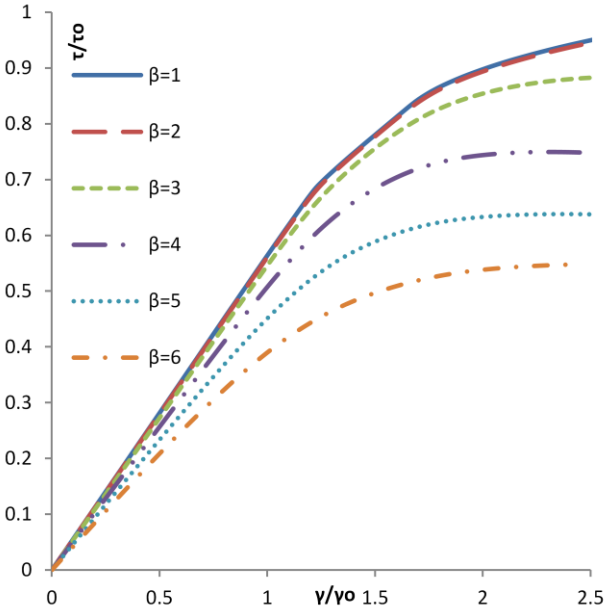

Figure 4. Shear stress-shear strain curves of aluminium alloy 5083-H116 plates with unrestrained edges under pure shear.

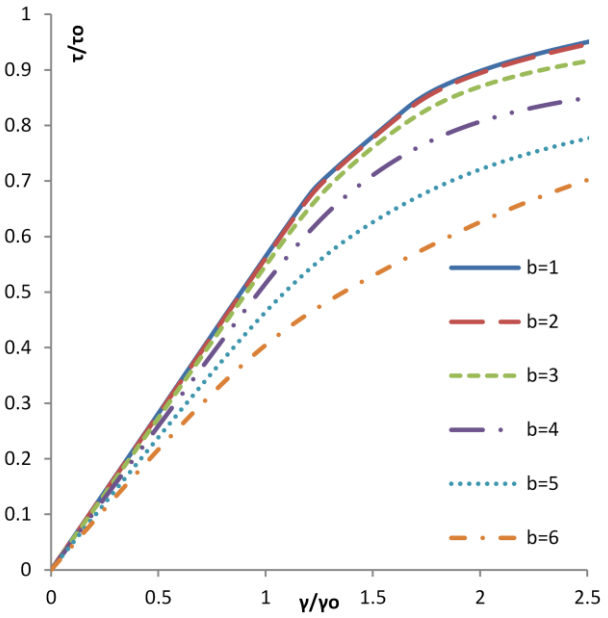

Figure 5. Shear stress-shear strain curves of aluminium alloy 5083-H116 plates with restrained edges under pure shear.

Figure 7 shows the graphs of the critical shear stress against plate slenderness (β) of the F.E. results for restrained and unrestrained plates under pure shear and according to Eurocode 9 (13) & (15). Stocky plates (b=1, 2) subjected to shear are also independent from the boundary conditions at the edges. The restrained slender plates withstand higher levels of critical shear stress than the unrestrained. However, the graphs for both boundary conditions have similar curvature.

Eurocode's 9 formula, (13), for non-slender plates estimates the critical shear stress due to yield. Additional, buckling check is required for slender plates using formula (15) for slender plates. The estimated critical shear stress for non-slender plates (β=1-2) according to Eurocode's 9 equation (13) is higher than the F.E. results but both graphs follow the same pattern, a straight horizontal line. The buckling shear stress of slender plates (β=3-6) derives from equation (15) and its graph shows similar tendency with our F.E. results.

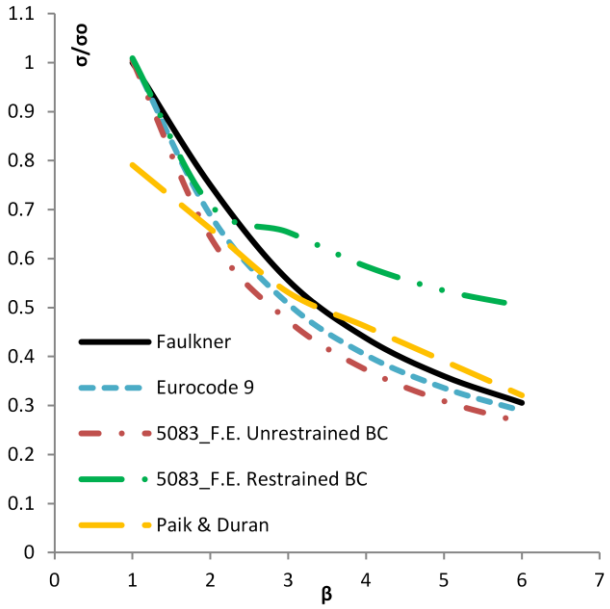

Figure 6. Comparison of F.E. results with theoretical formulas for aluminium alloy 5083-H116 plates under axial compression

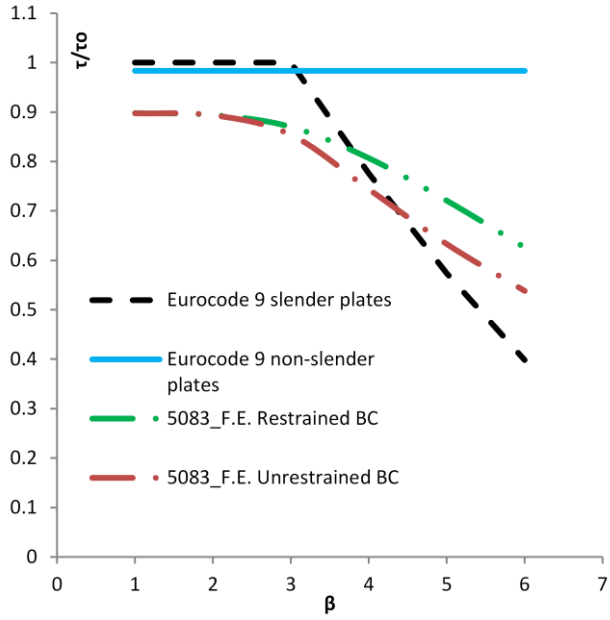

Figure 7. Comparison of F.E. results with theoretical formulas for aluminium alloy 5083-H116 plates under pure shear.

Figures 8 and 9 present the interaction diagram of axial compressive/tensile and shear loads for aluminium alloy 5083-H116 plates with unrestrained and restrained edges. Each point depicts the peak direct stress and the peak shear stress of plates under these combined loads. In cases where either the direct or shear stress components have failed to reach a peak value, limitations are set for the interaction relationship. In this case values of either direct or shear

stress at strain values of $\varepsilon/\varepsilon_o=2$ or $\gamma/\gamma_o=2$ are used to define the failure stresses for the interaction diagram.

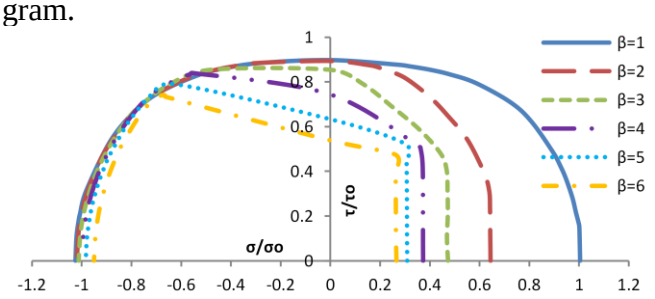

Figure 8. Interaction diagram of aluminium alloy 5083-H116 plates with unrestrained edges under axial compression and shear.

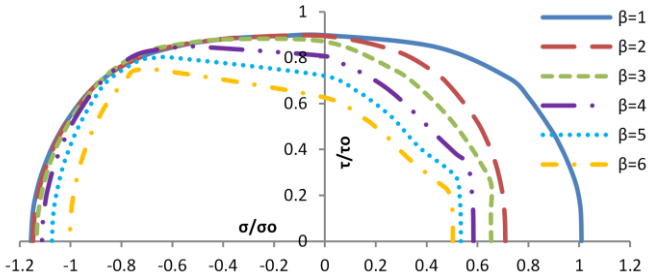

Figure 9. Interaction diagram of aluminium alloy 5083-H116 plates with restrained edges under axial compression and shear.

In Figure 8, the tensile direct stress is very close for all unrestrained plates (β=1-6), instead of the ultimate compressive stress which decreases depending on plate's slenderness ratio. Very stocky plates (β=1) follows the Mises yield criterion and very slender plates (β=3, 4, 5, 6) develop high insensitivity to shear. Buckling remains the dominate reason of failure for low proportions of shear to axial compressive load and shear starts to affect plate's strength when it reaches approximately the 50% of shear yield stress. The behaviour of plates with slenderness ratio β=2 is similar to the behaviour of stocky plates but without verifying the Mises yield criterion.

The interaction diagram of the restrained plates in Figure 9 has similar pattern with this of the unrestrained plates (Fig. 8). However, the restrained slender plates (β=2-6) present higher values of compressive and tensile stress. Very stocky plates β=1 comply with Mises criterion and less stocky plates β=2, 3 behave in a similar manner. The influence of shear load to the axial compressive strength is greater in slender plates (β=4, 5, 6) and shear buckling occurs for lower proportions of shear and more slender plates than in the unrestrained case.

4.2 *Alloy 6082-T6*

The equivalent graphs for aluminium alloy 6082-T6 plates with unrestrained and restrained edges have also been generated. These are presented in the following Figures 10-17, but because they are very similar to the aluminium alloy 5083-H116 results, only the differences between the two alloys will be analysed.

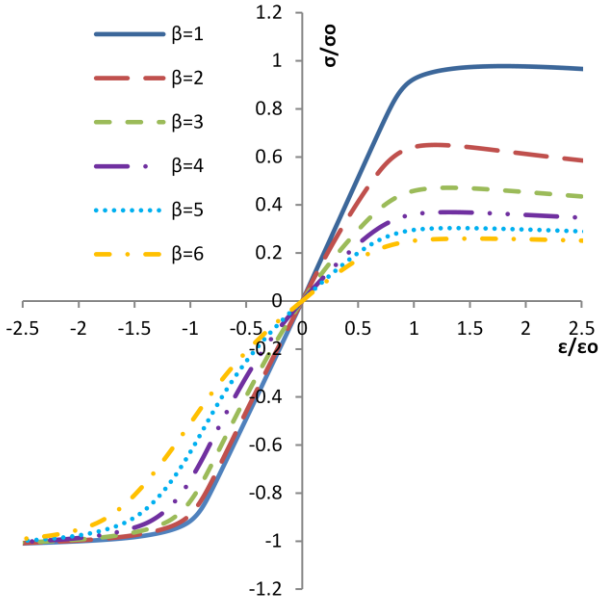

Figure 10. Stress-strain curves of aluminium alloy 6082-T6 plates with unrestrained edges under axial compression/tension.

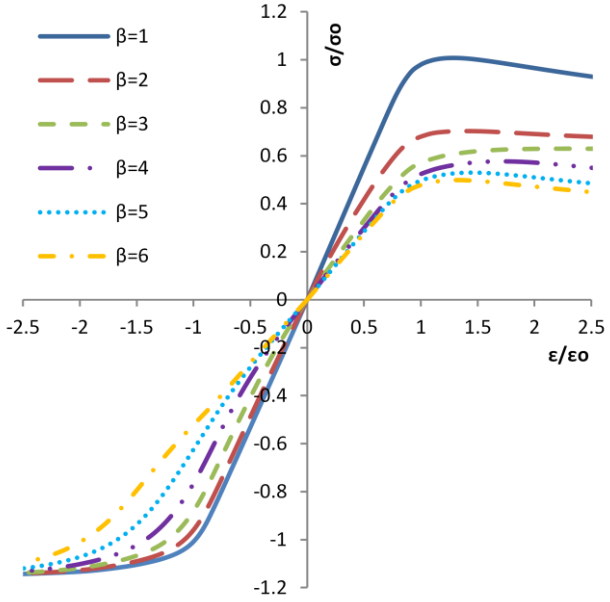

Figure 11. Stress-strain curves of aluminium alloy 6082-T6 plates with restrained edges under axial compression/tension.

Figures 10 and 11 show the load shortening curves for unrestrained and restrained plates respectively under axial compression and tension and there is no difference with Figures 2 and 3 for aluminium alloy 5083-H116.

Figures 12 and 13 show the shear stress-shear strain curves for aluminium alloy 6082-T6 plates with unrestrained and restrained edges and there is no noticeable difference with Figures 4 and 5 which depict the equivalent curves for aluminium alloy 5083-H116.

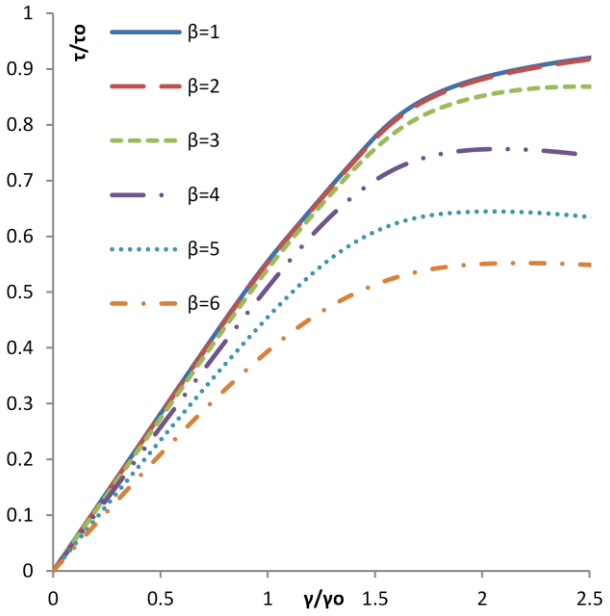

Figure 12. Shear stress-shear strain curves of aluminium alloy 6082-T6 plates with unrestrained edges under pure shear.

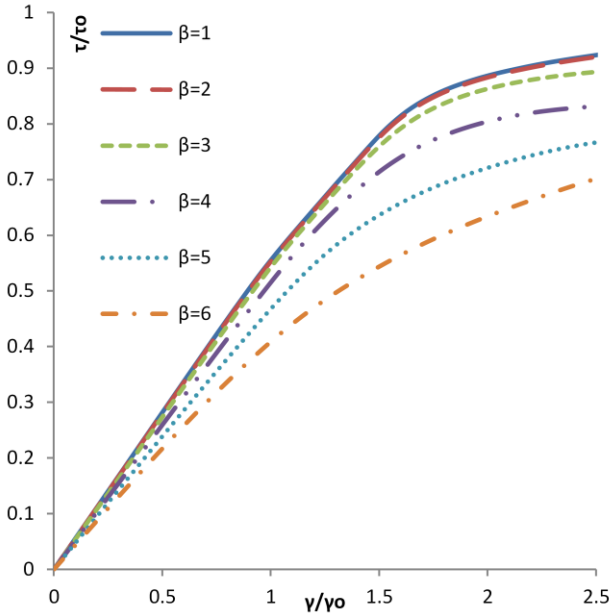

Figure 13. Shear stress-shear strain curves of aluminium alloy 6082-T6 plates with restrained edges under pure shear.

Since the results of the ultimate direct and critical shear stress for aluminium alloy 6082-T6 are very close to these for aluminium alloy 5083-H116, it is expected to generate similar graphs for the theoretical comparison. So, the graphs in Figures 14 and 15 in which the ultimate strength and the critical shear stress of our F.E. results are compared with theoretical formulas, actually verify the graphs in Figures 6 and 7.

The interaction diagram of axial compressive/tensile and shear loads for restrained aluminium alloy 6083-T6 (Fig. 17) is almost identical to the 5082-H116 diagram (Fig. 9). However, for unrestrained edges, the interaction diagrams of aluminium alloys 5083-H116 and 6082-T6 in Figure 8 and 16 are similar too, but slender plates (β=4, 5, 6) from alloy 6082-T6 present insensitivity of compressive strength to shear for lower proportions (40%) of the critical shear stress.

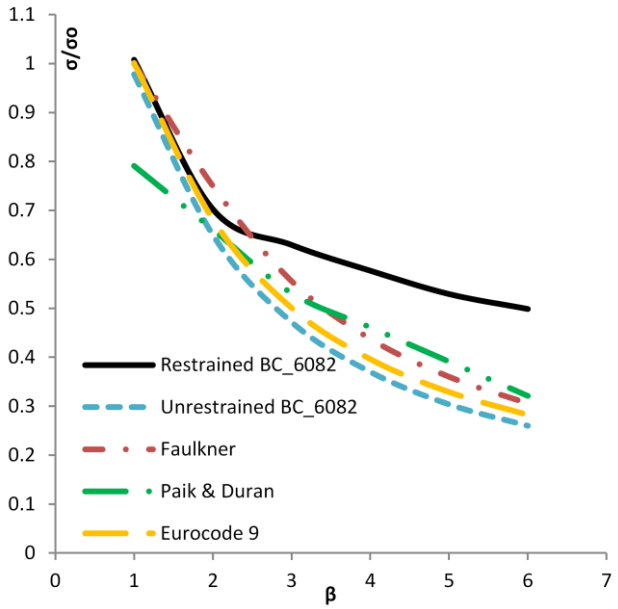

Figure 14. Comparison of F.E. results with theoretical formulas for aluminium alloy 6082-T6 plates under axial compression.

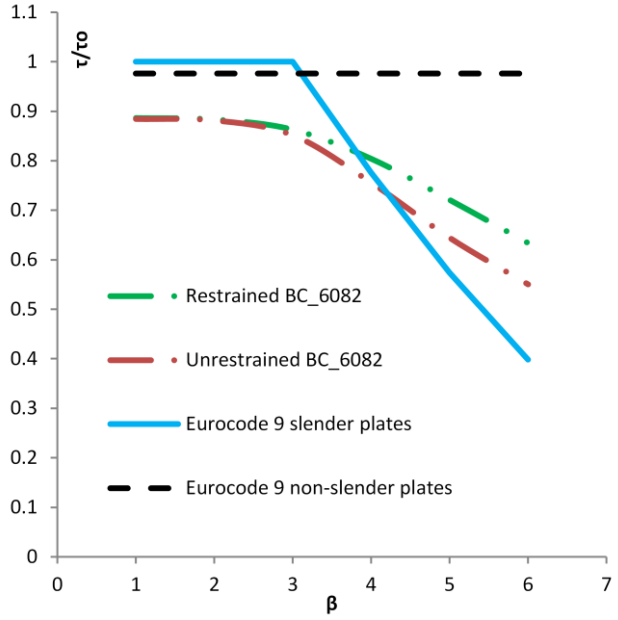

Figure 15. Comparison of F.E. results with theoretical formulas for aluminium alloy 6082-T6 plates under pure shear.

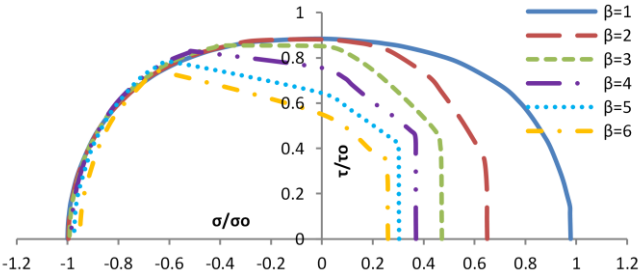

Figure 16. Interaction diagram of aluminium alloy 6082-T6 plates with unrestrained edges under axial compression and shear.

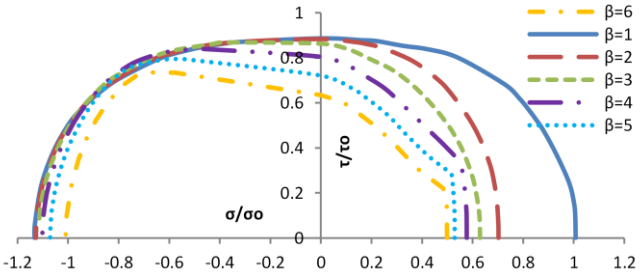

Figure 17. Interaction diagram of aluminium alloy 6082-T6 plates with restrained edges under axial compression and shear.

5 CONCLUSIONS

The results shown in the above figures serve to understand the behaviour of unrestrained and restrained aluminium alloys 5083-H116 and 6082-T6 plates under combined loads of axial compression/tension and shear. The main conclusions of this study are:

- The behaviour of very stocky plates (β=1) is independent from the constraints at their sides and follows the Mises yield criterion:
  $(\sigma/\sigma_o)^2 + (\tau/\tau_o)^2 = 1$
- Less stocky plates (β=2) independently from their constraints and restrained plates (β=3) have similar behaviour with stocky plates but without verifying the Mises yield criterion:
  $(\sigma/\sigma_o)^2 + (\tau/\tau_o)^2 < 1.$
- Slender plates β=4, 5, 6 with or without restrained edges and β=3 plates with unrestrained edges present insensitivity to low proportions of shear to axial load and in higher levels for the unrestrained case.
- All plates, except the very stocky β=1, sustain more direct and critical shear stress and become stiffer when their edges are restrained. Plate's strength depends directly on its slenderness ratio (β) for compressive loads, but it is not particularly affected by β for tensile loads.
- Both aluminium alloys 5083-H11 and 6082-T6 present very similar behaviour. The only remarkable notice is that aluminium alloy 6082-T6 slender unrestrained plates show insensitivity to shear for lower proportions of shear to axial load $0.4\tau_o$ than 5083-H116 plates.

6 ACKNOWLEDGEMENTS

This study was performed under an Office of Naval Research grant. We would like to thank ONR for their continuing support of this work.

7 REFERENCES

Alinia, M.M., Habashi, H.R., Khorram, A., 2009. Nonlinearity in the postbuckling behaviour of thin steel shear panels. Thin-Walled Struct. 47, 412–420.

Benson, S., 2011. Progressive Collapse Assessment of Lightweight Ship Structures. Newcastle University.

Chalmers, D.W., 1993. Design of Ships' Structures. HMSO, London.

DNV, 2001. Rules for Classification of High Speed, Light Craft and Naval Surface Craft. Det Norske Veritas.

Eurocode 3 ENV 1993-1-1, 2005. Design of steel structures, part 1.1 General rules and rules for buildings. British Standard Institution, London.

Eurocode 9 EN 1997-1-1, 2007. Design of Aluminium Structures, part 1.1 General structural rules. British Standard Institution, London.

Faulkner, D., 1975. A review of effective plating for use in the analysis of stiffened plating in bending and compression. J. Ship Res. 19, 1–17.

Frieze, P.A., Dowling, P.J., Hobbs, R.E., 1977. Ultimate Load Behaviour of Plates in Compression, in: Steel Plated Structures. Crosby Lockwood Staples, London, pp. 24–50.

Harding, J.E., Hobbs, R.E., Neal, B.G., 1977. Ultimate Load Behaviour of Plates under Combined Direct and Shear In-plane Loading, in: Steel Plated Structures. Crosby Lockwood Staples, London, pp. 369–404.

Mofflin, D., 1983. Plate Buckling in Steel and Aluminium. University of Cambridge.

Paik, J., Duran, A., 2004. Ultimate Strength of Aluminium Plates and Stiffened Panels for Marine Applications. Mar. Technol. Vol.41, 108–121.

Paik, J., Thayamballi, A., 2003. Ultimate limit state design of steel-plated structures. John Wiley & Sons Ltd, Chichester, UK.

Ramberg, W., Osgood, W.R., 1943. Description of stress-strain curves by three parameters. National Advisory Committee For Aeronautics, Washington DC.

Rizzo, N.A. dos S., Amante, D. do A., Estefen, S., 2014. Ultimate shear strength of stiffened panels for offshore structures, in: ASME 2014 33rd International Conference on Ocean, Offshore and Arctic Engineering. Presented at the OMAE 2014, San Francisco, California, USA.

Smith, C.S., 1977. Influence of local compressive failure on ultimate longitudinal strength of a ship's hull., in: Practical Design of Ships and Other Floating Structures. Presented at the Internatinal Symposium on Practical Design of Ships and Other Floating Structures., Tokyo, Japan.

Syrigou, M.S., Benson, S.D., Dow, R.S., 2014. Strength of Ship Plating under Combined Shear and Compression. Presented at the ASRANet, Glasgow.

Zhang, S., Kumar, P., Rutherford, S.E., 2008. Ultimate shear strength of plates and stiffened panels. Ships Offshore Struct. 3, 105–112.